Harmonic Reduction Methods at DC Link of Series-Connected Multi-Pulse Rectifiers: A Review

Qingxiao Du, Lei Gao, Quanhui Li, Wei Liu, Xinyu Yin, and Fangang Meng, *Member, IEEE*

***Abstract*—Series-connected multipulse rectifiers (MPRs) are used to provide high-quality electric power for high-voltage and high-power occasions. Due to conventional MPRs have limited harmonic reduction ability that cannot fulfill the related harmonic standard, some effective dc side harmonic reduction methods have been proposed to further improve power quality of the MPRs. This article gives a comprehensive review on dc link harmonic reduction methods of series-connected MPRs. Passive and active harmonic reduction mechanisms are respectively analyzed based on two typical topologies, which are theoretical foundations for understanding and constructing novel harmonic reduction circuits (HRCs). Some useful dc side HRCs are presented and compared from aspects of their performances, complexity of the overall structure, magnetic device capacity and power losses, etc. The necessary simulation results are given to verify and compare the effectiveness of some involved harmonic reduction methods. Based on these topologies, the advantages, drawbacks and future trends of the passive or active methods are concluded; besides, the hybrid harmonic reduction methods are also considered. This article aims to provide useful guidance for the researches of harmonic elimination and multipulse rectification technology.**

***Index Terms*—DC link harmonic reduction method, harmonic reduction mechanism, input current THD, series-connected multipulse rectifier (MPR).**

I. Introduction

WITH RAPID developments of power semiconductor devices, rectifiers as one of the main power conversion devices have been widely used in power systems, industrial and agricultural production occasions as well as transportation and aerospace fields [1]. Meanwhile, it cannot be ignored that rectifiers also bring serious harmonic pollutions due to their properties of nonlinearity and time variability, both voltage and current harmonics in grid cause damage to grid itself and even do harm to electrical equipment connected to gird [2]. Therefore, it is an essential work to do researches on harmonic reduction methods.

In general, there are two kinds of methods to deal with harmonics caused by rectifiers. One method is to install suitable passive or active filters to compensate harmonics, which has functions to eliminate harmonics at specific frequencies for all kinds of harmonic sources; while in many cases, this method leads to high economic costs and power losses, further more with system's components number increases, its overall reliability is reduced [3]. However, compared with filters, reconstruct rectifiers is a more attractive method that can fundamentally deal with harmonic pollutions [4], [5]. This method can also be divided into two kinds, in low and medium power occasions, pulsewidth modulation (PWM) rectifiers have a broad utilization [6]; while multipulse rectifiers (MPRs) are more suitable for high power occasions that can reduce power losses [7]. Besides, PWM rectifiers need more complex measurement and feedback control circuits. Take all factors into account, MPRs have wider prospects due to their high robustness. Whether it is a series-connected MPR or a parallel-connected MPR, its harmonic reduction performance mainly depends on the pulse number of the rectifier. After using dc side harmonic reduction circuits (HRCs), higher pulse number and better performances can be obtained [8]–[24]. Compared with parallel-connected MPRs, series connection of bridge rectifiers can achieve higher output voltages, so that series-connected MPRs extend MPR's utilizations to higher voltage and higher power fields [25]–[45]. In addition, series connection avoids current imbalance phenomenon, which may occur in parallel-connected MPRs and cause adverse influence on actual harmonic reduction performances.

In recent decades, related institutions and scholars have proposed some dc side harmonic reduction methods of parallel-connected MPRs [1], but there are less novel MPRs are concentrated on series-connected forms, this is due to that dc side HRCs of parallel-connected MPRs have more clear design mechanisms and implementation methods. In order to promote future researches on novel series-connected MPRs and discover their potentials, it is essential to do comprehensive derivations on harmonic reduction mechanisms of series-connected MPRs and compare their characteristics.

In this article, according to whether there are filter inductors at ac side, series-connected MPRs can be generally divided into current source rectifiers and voltage source rectifiers, and their dc side harmonic reduction methods both include passive and active methods. First, this article clarifies the passive and active harmonic reduction mechanisms of dc side harmonic reduction methods. Furthermore, characteristics of some effective passive, active and hybrid HRCs from aspects of power quality, total kVA rating of the magnetic devices, suitable occasions and realizable complexity are respectively presented in Sections III–V. In

Manuscript received June 15, 2021; revised September 13, 2021; accepted September 30, 2021. Date of publication October 6, 2021; date of current version November 30, 2021. This work was supported in part by the National Natural Foundation of China under Grant 51777042. Recommended for publication by Associate Editor M. Hagiwara. *(Corresponding author: Fangang Meng.)*

The authors are with the School of Electrical Engineering and Automation, Harbin Institute of Technology, Harbin 150001, China (e-mail: 690384469@qq.com; hualeier111@126.com; a875921420@qq.com; l61847@163.com; yxy06281205@163.com; mfg0327@sina.com).

Color versions of one or more figures in this article are available at https://doi.org/10.1109/TPEL.2021.3118040.

Digital Object Identifier 10.1109/TPEL.2021.3118040

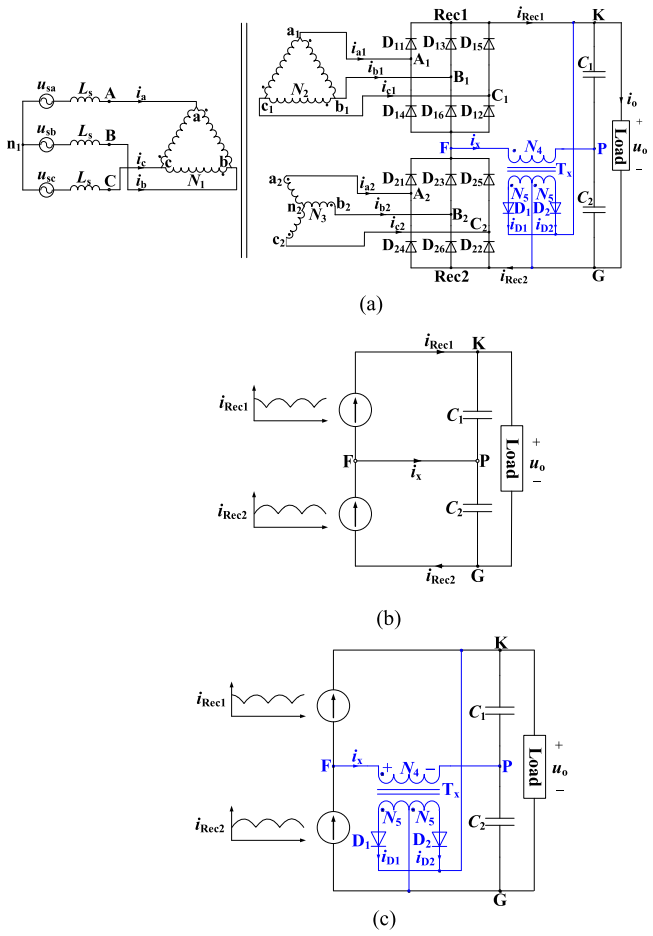

Fig. 1. Series-connected 24-pulse rectifier with dc side passive HRC. (a) Main topology of the 24-pulse rectifier. (b) Equivalent model of the 24-pulse rectifier when the single-phase rectifier is not working. (c) Equivalent model of the 24-pulse rectifier when the single-phase rectifier is working.

addition, simulation verifications are presented in Section VI, and future trends are also concluded in Section VII. All above works have not been done in previous papers. Therefore, this article is aimed at providing comprehensive and clear guidelines for HRC selection and research.

II. Harmonic Reduction Mechanism Analysis

In this section, based on current source rectifiers, the passive and active harmonic reduction mechanisms of the series-connected MPRs are presented in detail, which are helpful for understanding the operation principles of the mentioned dc side HRCs in the following sections.

A. Passive Harmonic Reduction Mechanism Analysis

As shown in Fig. 1(a) [25], this series-connected 24-pulse rectifier is taken as an example to clarify passive harmonic reduction mechanism. The main circuit is a 12-pulse rectifier, and dc side passive HRC is consisted with a single-phase transformer (T_x) and a single-phase full-wave bridge rectifier. Based on Fig. 1(a), the model when the dc side HRC is not working [see Fig. 1(b)]

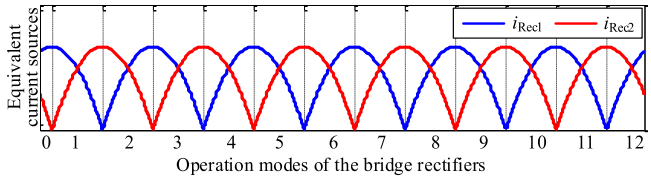

Fig. 2. Waveforms of the equivalent current sources i_{Rec1} and i_{Rec2}.

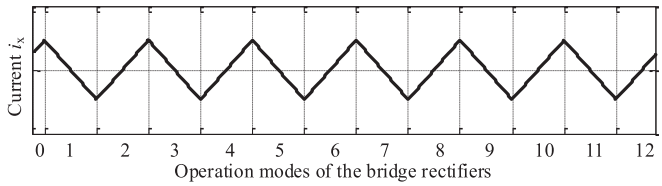

Fig. 3. Waveform of the current difference i_{x}.

can be established to clarify the operation modes of the main circuit, and form comparisons to the 24-pulse rectification state [see Fig. 1(c)].

Assume that the voltages provided by the voltage sources are

$$\begin{cases} u_{\mathrm{a}} = \sqrt{2}E\sin\omega t \\ u_{\mathrm{b}} = \sqrt{2}E\sin(\omega t - 2\pi/3) \\ u_{\mathrm{c}} = \sqrt{2}E\sin(\omega t + 2\pi/3) \end{cases} \tag{1}$$

where E is the RMS value of the input voltages.

If the turns ratio of the $\Delta/\Delta/Y$ phase-shifting transformer is $N_1 : N_2 : N_3 = K\sqrt{3} : \sqrt{3} : 1$, the input voltages of the phase-shifting transformer can be presented as

$$\begin{cases} u_{an1} \approx \frac{\sqrt{2}E}{K}\sin(\omega t - \varphi) \\ u_{bn1} \approx \frac{\sqrt{2}E}{K}\sin(\omega t - 2\pi/3 - \varphi) \\ u_{cn1} \approx \frac{\sqrt{2}E}{K}\sin(\omega t + 2\pi/3 - \varphi) \end{cases} \tag{2}$$

where φ is the phase difference between ac voltage sources and input currents.

Due to the existence of inductors L_{s}, in combination with the configuration of the phase-shifting transformer, the three-phase bridge rectifiers Rec1 and Rec2 can be replaced by two current sources with the same RMS value and a phase difference of 30°. In Fig. 1(b), midpoints F and P are connected to provide a conductive path for current difference of i_{Rec1} and i_{Rec2}; and in Fig. 1(c), the HRC is consistent with the original circuit.

The waveforms of current sources i_{Rec1} and i_{Rec2} are shown in Fig. 2, and Table I gives diode operation modes in each interval. Based on Fig. 2 and Kirchhoff's current law (KCL), the waveform of current difference i_{x} can be plotted as shown in Fig. 3, which determines the operation modes of the passive HRC. When $i_{\mathrm{x}} > 0$, current flows into the dotted terminal of the primary side, and flows out of the secondary side of T_x, diode D_1 is forward-biased and turned ON (mode I); on the contrary, when $i_{\mathrm{x}} < 0$, current flows out of the dotted terminal of the primary side, and flows into the secondary side of T_x, diode D_2 is forward-biased and turned ON (mode II). Defining that the turns ratio n of T_x is N_1: N_2. Through alternative conduction

TABLE I
OPERATION MODES OF THE THREE-PHASE BRIDGE RECTIFIERS

Mode	Interval	i_{Rec1}	i_{Rec2}	Conductive Diodes
0	[0, φ)	i_{c1b1}	i_{c2b2}	D_{15} D_{16} D_{25} D_{26}
1	[φ, φ+30°)	i_{c1b1}	i_{a2b2}	D_{15} D_{16} D_{21} D_{26}
2	[φ+30°, φ+60°)	i_{a1b1}	i_{a2b2}	D_{11} D_{16} D_{21} D_{26}
3	[φ+60°, φ+90°)	i_{a1b1}	i_{a2c2}	D_{11} D_{16} D_{21} D_{22}
4	[φ+90°, φ+120°)	i_{a1c1}	i_{a2c2}	D_{11} D_{12} D_{21} D_{22}
5	[φ+120°, φ+150°)	i_{a1c1}	i_{b2c2}	D_{11} D_{12} D_{23} D_{22}
6	[φ+150°, φ+180°)	i_{b1c1}	i_{b2c2}	D_{13} D_{12} D_{23} D_{22}
7	[φ+180°, φ+210°)	i_{b1c1}	i_{b2a2}	D_{13} D_{12} D_{23} D_{24}
8	[φ+210°, φ+240°)	i_{b1a1}	i_{b2a2}	D_{13} D_{14} D_{23} D_{24}
9	[φ+240°, φ+270°)	i_{b1a1}	i_{c2a2}	D_{13} D_{14} D_{25} D_{24}
10	[φ+270°, φ+300°)	i_{c1a1}	i_{c2a2}	D_{15} D_{14} D_{25} D_{24}
11	[φ+300°, φ+330°)	i_{c1a1}	i_{c2b2}	D_{15} D_{14} D_{25} D_{26}
12	[φ+330°, 360°)	i_{c1b1}	i_{c2b2}	D_{15} D_{16} D_{25} D_{26}

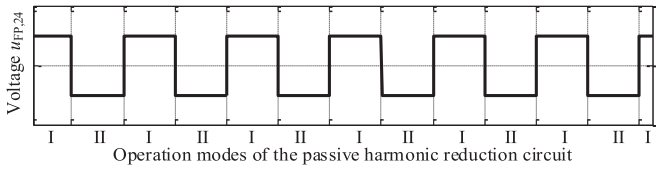

Fig. 4. Waveform of the voltage $u_{\mathrm{FP,24}}$.

TABLE II
OPERATION MODES OF THE PASSIVE HRC

Mode	Interval	Mode	Interval
I	[0, φ+15°)	I	[φ+165°, φ+195°)
II	[φ+15°, φ+45°)	II	[φ+195°, φ+225°)
I	[φ+45°, φ+75°)	I	[φ+225°, φ+255°)
II	[φ+75°, φ+105°)	II	[φ+255°, φ+285°)
I	[φ+105°, φ+135°)	I	[φ+285°, φ+315°)
II	[φ+135°, φ+165°)	II	[φ+315°, φ+345°)
		I	[φ+345°, 360°)

of diodes D_1 and D_2, the square-wave voltage $u_{\mathrm{FP,24}}$ with the amplitude of $n(u_{\mathrm{o}}+U_d)$ is formed as shown in Fig. 4, which can further influence step number and level values of input voltage u_{An1}. Table II is the corresponding intervals of modes I and II.

In combination with Fig. 1, the relationship between primary and secondary side voltages of the phase-shifting transformer satisfies that

$$\begin{cases} u_{\mathrm{An1}} = \frac{1}{\sqrt{3}} u_{\mathrm{A1B1}} \angle -\frac{\pi}{6} \\ u_{\mathrm{A1B1}} = u_{\mathrm{AB}} = \sqrt{3} u_{\mathrm{A2n2}} \\ u_{\mathrm{B1C1}} = u_{\mathrm{BC}} = \sqrt{3} u_{\mathrm{B2n2}}. \end{cases} \tag{3}$$

Taking points "*P*" and "*G*" as the reference points of Rec1 and Rec2, respectively. Based on Kirchhoff's voltage law (KVL), it

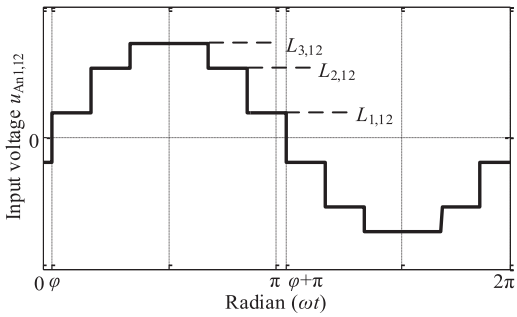

Fig. 5. Waveform of the input voltage $u_{\mathrm{An1,12}}$.

can be obtained that

$$\begin{cases} u_{\mathrm{A2n2}} = u_{\mathrm{A2G}} - u_{\mathrm{n2G}} \\ u_{\mathrm{B2n2}} = u_{\mathrm{B2G}} - u_{\mathrm{n2G}} \\ u_{\mathrm{C2n2}} = u_{\mathrm{C2G}} - u_{\mathrm{n2G}}. \end{cases} \tag{4}$$

Under balanced conditions, the following relation is established:

$$u_{\mathrm{A2n2}} + u_{\mathrm{B2n2}} + u_{\mathrm{C2n2}} = 0. \tag{5}$$

From (4) and (5), voltage u_{n2G} can be expressed as

$$u_{\mathrm{n2G}} = \frac{u_{\mathrm{A2G}} + u_{\mathrm{B2G}} + u_{\mathrm{C2G}}}{3}. \tag{6}$$

When the single-phase rectifier in the HRC is not working, the rectifier shown in Fig. 1 is operating under the 12-pulse rectification state. For the series-connected 12-pulse rectifier, its input voltage is determined by operation modes of main circuit as given in Table I. Taking Mode 1 as an example to clarify formation process of voltage $u_{\mathrm{An1,12}}$. In mode 1, the following voltages can be directly obtained:

$$\begin{cases} u_{\mathrm{B1P,12}} = -U_{\mathrm{d}} \\ u_{\mathrm{C1P,12}} = \frac{u_{\mathrm{o}}}{2} + U_{\mathrm{d}} \end{cases} \quad \begin{cases} u_{\mathrm{A2G,12}} = \frac{u_{\mathrm{o}}}{2} + U_{\mathrm{d}} \\ u_{\mathrm{B2G,12}} = -U_{\mathrm{d}} \end{cases} \tag{7}$$

where U_d is the diode conduction voltage drop and u_{o} is the load voltage.

From (3) and (7), voltages $u_{\mathrm{A1P,12}}$ and $u_{\mathrm{C2G,12}}$ can be obtained

$$\begin{cases} u_{\mathrm{A1P,12}} = \frac{\sqrt{3}-1}{2} u_{\mathrm{o}} + (2\sqrt{3}-3) U_{\mathrm{d}} \\ u_{\mathrm{C2G,12}} = \frac{\sqrt{3}-1}{2} u_{\mathrm{o}} + (2\sqrt{3}-3) U_{\mathrm{d}}. \end{cases} \tag{8}$$

According to (7) and (8), $u_{\mathrm{A1B1,12}}$ is

$$u_{\mathrm{A1B1,12}} = \frac{\sqrt{3}-1}{2}(u_{\mathrm{o}} + 4U_d). \tag{9}$$

From relations in (3), $u_{\mathrm{An1,12}}$ is

$$u_{\mathrm{An1,12}} = \frac{\sqrt{3}-1}{2\sqrt{3}}(u_{\mathrm{o}} + 4U_d). \tag{10}$$

Similarly, other levels of $u_{\mathrm{An1,12}}$ can be calculated, Fig. 5 is the theoretical waveform of $u_{\mathrm{An1,12}}$, and Table III gives level values of $u_{\mathrm{An,12}}$.

For the series-connected 24-pulse rectifier as shown in Fig. 1, its overall operation mode is a combination of operation modes of main circuit and dc side passive HRC. Based on Tables I and

TABLE III
LEVEL VALUES OF THE VOLTAGE $u_{\mathrm{An1,12}}$

Voltage	Level Value
$L_{1,12}$	$\frac{2-\sqrt{3}}{2\sqrt{3}}(u_o+4U_d)$
$L_{2,12}$	$\frac{\sqrt{3}-1}{2\sqrt{3}}(u_o+4U_d)$
$L_{3,12}$	$\frac{1}{2\sqrt{3}}(u_o+4U_d)$

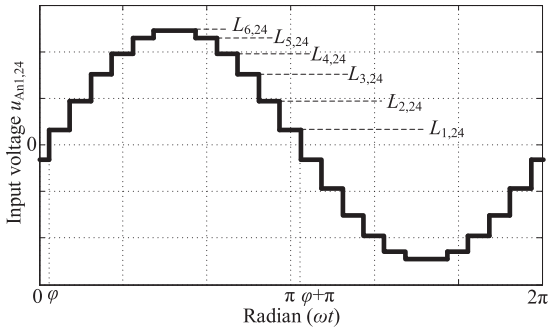

Fig. 6. Waveform of the input voltage $u_{\mathrm{An1,24}}$.

TABLE IV
LEVEL VALUES OF THE VOLTAGE $u_{\mathrm{An1,24}}$

Voltage	Level Value
$L_{1,24}$	$\frac{2-\sqrt{3}}{2\sqrt{3}}(u_o+4U_d)-\frac{(2+\sqrt{3})N_4}{\sqrt{3}N_5}(u_o+U_d)$
$L_{2,24}$	$\frac{2-\sqrt{3}}{2\sqrt{3}}(u_o+4U_d)+\frac{(2+\sqrt{3})N_4}{\sqrt{3}N_5}(u_o+U_d)$
$L_{3,24}$	$\frac{\sqrt{3}-1}{2\sqrt{3}}(u_o+4U_d)-\frac{(\sqrt{3}+1)N_4}{\sqrt{3}N_5}(u_o+U_d)$
$L_{4,24}$	$\frac{\sqrt{3}-1}{2\sqrt{3}}(u_o+4U_d)+\frac{(\sqrt{3}+1)N_4}{\sqrt{3}N_5}(u_o+U_d)$
$L_{5,24}$	$\frac{1}{2\sqrt{3}}(u_o+4U_d)-\frac{N_4}{\sqrt{3}N_5}(u_o+U_d)$
$L_{6,24}$	$\frac{1}{2\sqrt{3}}(u_o+4U_d)+\frac{N_4}{\sqrt{3}N_5}(u_o+U_d)$

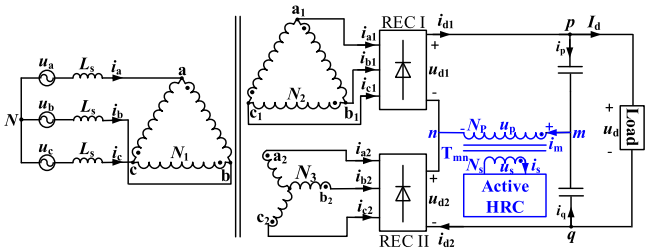

Fig. 7. Series-connected 12-pulse rectifier with DC side active HRC (current source type).

II, taking operation modes in interval $[\varphi, \varphi+15^{\mathrm{o}})$ as an example to clarify formation process of voltage $u_{\mathrm{An1,24}}$. In this interval, the following voltages can be directly obtained:

$$\begin{cases} u_{\mathrm{B1P,24}} = -u_{\mathrm{x}} - U_d \\ u_{\mathrm{C1P,24}} = \frac{u_{\mathrm{o}}}{2} + U_d \end{cases} \begin{cases} u_{\mathrm{A2G,24}} = \frac{u_{\mathrm{o}}}{2} - u_x + U_d \\ u_{\mathrm{B2G,24}} = -U_d \end{cases} \tag{11}$$

where u_{x} is the amplitude of the square-wave voltage u_{FP}.

From (3) and (11), voltages $u_{\mathrm{A1P,24}}$ and $u_{\mathrm{C2G,24}}$ can be obtained

$$\begin{cases} u_{\mathrm{A1P,24}} = \frac{\sqrt{3}-1}{2}u_{\mathrm{o}} - (2+\sqrt{3})u_x + (2\sqrt{3}-3)U_d \\ u_{\mathrm{C2G,24}} = \frac{\sqrt{3}-1}{2}u_{\mathrm{o}} + (\sqrt{3}+1)u_x + (2\sqrt{3}-3)U_d. \end{cases} \tag{12}$$

According to (11) and (12), $u_{\mathrm{A1B1,24}}$ is

$$u_{\mathrm{A1B1,24}} = \frac{\sqrt{3}-1}{2}(u_{\mathrm{o}}+4U_d) - (\sqrt{3}+1)u_x. \tag{13}$$

From relations in (3), $u_{\mathrm{An1,24}}$ is

$$u_{\mathrm{An1,24}} = \frac{\sqrt{3}-1}{2\sqrt{3}}(u_{\mathrm{o}}+4U_d) - \frac{(\sqrt{3}+1)N_4}{\sqrt{3}N_5}(u_{\mathrm{o}}+U_d). \tag{14}$$

Similarly, other levels of $u_{\mathrm{An1,24}}$ can be calculated, Fig. 6 is the theoretical waveform of $u_{\mathrm{An1,24}}$, and Table IV gives level values of $u_{\mathrm{An,24}}$. In [11], it indicates that the optimum turns ratio n is 55.8 under the minimum total harmonic distortion (THD) value of input voltages.

The basic harmonic reduction mechanism of the passive HPR is increasing operation modes of the rectifier, that is indirectly increasing the step number of the input voltage. As the step number of input voltage increases, high-content low-order harmonics can be suppressed, thereby improving the power quality of the input current. However, the harmonic reduction ability of the passive HRC is limited; besides, the power factor may decrease since the phase angle between the input current and the voltage source cannot be eliminated. It is necessary to use active HRC to further improve power quality.

B. Active Harmonic Reduction Mechanism Analysis

In previous pieces of literature, especially for the current source rectifier, the harmonic reduction mechanism of dc side active harmonic reduction method lacks accuracy, and the theoretical derivation of the modulation current waveform is not given. In this paper, the active harmonic reduction mechanism is clearly presented based on the 12-pulse rectifier shown in Fig. 7. In Fig. 7, the main circuit of the MPR is same as that in Fig. 1, and the dc side active HRC is consisted with a single-phase transformer T_{mn} and the circuit connected with the secondary side of T_{mn}, this auxiliary circuit can be any controllable circuit that can generate the needed current waveform.

In order to eliminate the phase difference φ and improve the power factor, the current provided by the active HRC should be determined under the premise of ignoring the influence of phase difference. Therefore, in theoretical analysis, the voltage source type rectifier shown in Fig. 8 is used to replace the current source type rectifier in Fig. 7.

Compared with Fig. 7, the rectifier shown in Fig. 8 without using ac side filter inductance. It is necessary to add a single-phase transformer T_{pq} between the two dc side capacitors to ensure that the effective values of the currents flowing through

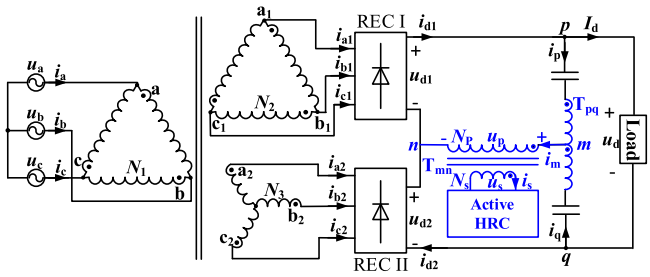

Fig. 8. Series-connected 12-pulse rectifier with dc side active HRC (voltage source type).

the two capacitors are equal. The rest parts are consistent with Fig. 7.

Based on the configuration of the phase-shifting transformer and (2), the output voltages of the phase-shifting transformer are

$$\begin{cases} u_{a1} = \frac{\sqrt{2}E}{K}\sin\omega t \\ u_{b1} = \frac{\sqrt{2}E}{K}\sin(\omega t - 2\pi/3) \\ u_{c1} = \frac{\sqrt{2}E}{K}\sin(\omega t + 2\pi/3) \end{cases} \quad \begin{cases} u_{a2} = \frac{\sqrt{2}E}{K}(\sin\omega t + \pi/6) \\ u_{b2} = \frac{\sqrt{2}E}{K}\sin(\omega t - \pi/2) \\ u_{c2} = \frac{\sqrt{2}E}{K}\sin(\omega t + 5\pi/6). \end{cases} \tag{15}$$

According to the operation principle of three-phase bridge rectifiers, the output voltages of the two sets of three-phase bridge rectifiers can be obtained

$$\begin{cases} u_{d1} = S_{a1}u_{a1} + S_{b1}u_{b1} + S_{c1}u_{c1} \\ u_{d2} = S_{a2}u_{a2} + S_{b2}u_{b2} + S_{c2}u_{c2} \end{cases} \tag{16}$$

where $S_{a1}, S_{b1}, S_{c1}, S_{a2}, S_{b2,}$ and S_{c2} are the switching functions of phases "$a1$," "b1," "$c1$," "$a2$," "b2," and "c2," respectively.

The switching function S_{a1} can be expressed as

$$S_{a1} = \frac{1}{2}\left\{\mathrm{sgn}\left[u_{a1} - u_{c1}\right] - \mathrm{sgn}\left[u_{b1} - u_{a1}\right]\right\}. \tag{17}$$

Each switching function satisfies the following relations:

$$\begin{cases} S_{b1} = S_{a1}\angle - 2\pi/3 \\ S_{c1} = S_{a1}\angle + 2\pi/3 \end{cases} \quad \begin{cases} S_{a2} = S_{a1}\angle + \pi/6 \\ S_{b2} = S_{a1}\angle - \pi/2 \\ S_{c2} = S_{a1}\angle + 5\pi/6. \end{cases} \tag{18}$$

According to KVL, the load voltage u_d is

$$u_d = u_{d1} + u_{d2} \tag{19}$$

where u_{d1} and u_{d2} are the output voltages of rectifiers REC I and REC II.

From (15) to (19), the expression of u_d in the domain $[0, +\infty)$ can be obtained as follows:

$$u_d = \frac{E}{K}\sqrt{12 + 6\sqrt{3}}\sin\left(\omega t + \frac{5\pi}{12}\right) \omega t \in \left[\frac{k\pi}{6}, \frac{k\pi}{3}\right) \tag{20}$$

where k is a positive integer.

According to the operating principle of three-phase rectifier bridge, the 6-phase output current of the transformer can be written as

$$\begin{cases} i_{a1} = S_{a1}i_{d1} \\ i_{b1} = S_{b1}i_{d1} \\ i_{c1} = S_{c1}i_{d1} \end{cases} \quad \begin{cases} i_{a2} = S_{a2}i_{d2} \\ i_{b2} = S_{b2}i_{d2} \\ i_{c2} = S_{c2}i_{d2}. \end{cases} \tag{21}$$

where i_{d1} and i_{d2} are output currents of rectifiers REC I and REC II.

According to KCL and ampere-turn balance principle, the primary side currents of the isolated transformer are

$$\begin{cases} i_a = \frac{N_2}{N_1}i_{a1} + \frac{N_3}{N_1}(i_{a2} - i_{c2}) \\ i_b = \frac{N_2}{N_1}i_{b1} + \frac{N_3}{N_1}(i_{b2} - i_{a2}) \\ i_c = \frac{N_2}{N_1}i_{c1} + \frac{N_3}{N_1}(i_{c2} - i_{b2}). \end{cases} \tag{22}$$

Under the condition of large inductive load, i_{d1} and i_{d2} can be obtained by KCL and Fig. 8

$$\begin{cases} i_{d1} = I_d + i_p \\ i_{d2} = I_d - i_q \end{cases} \tag{23}$$

where I_d is the load current, i_p and i_q satisfies

$$i_p = i_q = \frac{1}{2}i_m. \tag{24}$$

Substituting (21), (23), and (24) into (22), the input current of the rectifier can be obtained

$$\begin{cases} i_a = \frac{S_{a1}}{K}\left(I_d + \frac{1}{2}i_m\right) + \frac{1}{K\sqrt{3}}(S_{a2} - S_{c2})(I_d - \frac{1}{2}i_m) \\ i_b = \frac{S_{b1}}{K}\left(I_d + \frac{1}{2}i_m\right) + \frac{1}{K\sqrt{3}}(S_{b2} - S_{a2})(I_d - \frac{1}{2}i_m) \\ i_c = \frac{S_{c1}}{K}\left(I_d + \frac{1}{2}i_m\right) + \frac{1}{K\sqrt{3}}(S_{c2} - S_{b2})(I_d - \frac{1}{2}i_m). \end{cases} \tag{25}$$

From (25), it can be observed that when the current i_m meets a certain condition, the input current of the rectifier will not contain harmonics. Taking phase "a" as an example, the current i_m can be expressed as

$$i_{am} = \frac{Ki_a - S_{a1}I_d - \frac{1}{\sqrt{3}}(S_{a2} - S_{c2})I_d}{\frac{1}{2}S_{a1} - \frac{1}{2\sqrt{3}}(S_{a2} - S_{c2})}. \tag{26}$$

Assume that the waveform of i_a is a standard sine wave, that is

$$i_a = \sqrt{2}I_{a,1}\sin\omega t \tag{27}$$

where $I_{a,1}$ is the effective value of fundamental wave of i_a.

According to the power conservation law, the relationship between input and output power of the system can be established

$$3EI_{a,1} = U_dI_d \tag{28}$$

where U_d is the effective value of the load voltage.

Before and after equivalent substitution, only the phase difference of load voltage changes, while the effective value remains unchanged. It can be obtained from (8) that

$$U_d = \frac{E}{K}\sqrt{\frac{(6 + 3\sqrt{3})(\pi + 3)}{\pi}}. \tag{29}$$

Substituting (29) into (28), it can be obtained that

$$I_{a,1} = \frac{I_d}{3K}\sqrt{\frac{(6 + 3\sqrt{3})(\pi + 3)}{\pi}}. \tag{30}$$

Then substituting (30) into (27), the current i_a can be rewritten as

$$i_a \approx 2.2054\frac{I_d}{K}\sin\omega t. \tag{31}$$

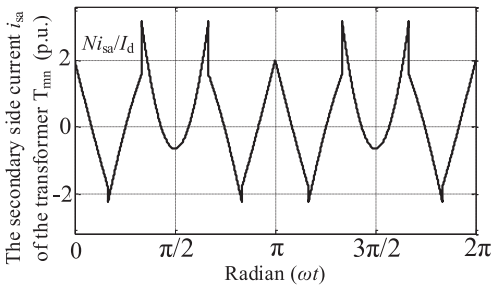

Fig. 9. Secondary side current i_{sa} of the transformer T_{mn}.

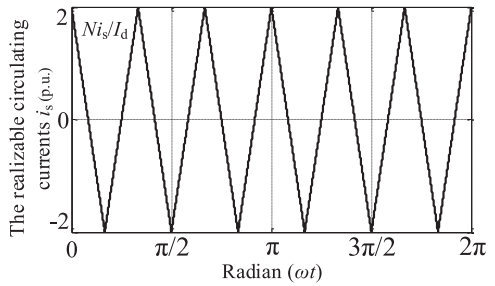

Fig. 10. Realizable circulating currents i_s.

Substituting (31) into (26), the needed current i_m can be obtained, in a real circuit, the control of current i_m is often achieved by controlling the secondary side current i_s.

The primary and secondary side current relationship of transformer T_{mn} is

$$i_s = \frac{N_p}{N_s} i_m. \tag{32}$$

In combination with (26), (31) and (32), we can get

$$\frac{i_{sa}}{I_d} = \frac{N_p}{N_s} \frac{2.2054 \sin \omega t - S_{a1} - \frac{1}{\sqrt{3}}(S_{a2} - S_{c2})}{\frac{1}{2} S_{a1} - \frac{1}{2\sqrt{3}}(S_{a2} - S_{c2})}. \tag{33}$$

When N_p: N_s is 1: N, the waveform of Ni_{sa}/I_d is shown in Fig. 9, and the current i_a is a pure sinusoidal wave.

When the three-phase input currents are all standard sine waves, the required circulations i_{sa}, i_{sb}, and i_{sc} are asymmetrical triangular waves with phase difference of 120°, but only one waveform can exist on the secondary side of the injection transformer. Therefore, the asymmetrical triangular wave can be approximated to the realized symmetrical triangular wave i_s as shown in Fig. 10, which is injected into the secondary side of the transformer T_{mn}.

When the waveform of the auxiliary side current of the harmonic injection transformer is shown in Fig. 10, the waveforms of currents i_{d1} and i_{d2} are plotted as shown in Fig. 11, the waveforms of currents i_{a1}, i_{a2}, and $-i_{c2}$ can be plotted as shown in Fig. 12, and the three-phase input currents are approximated to sine waves, as shown in Fig. 13.

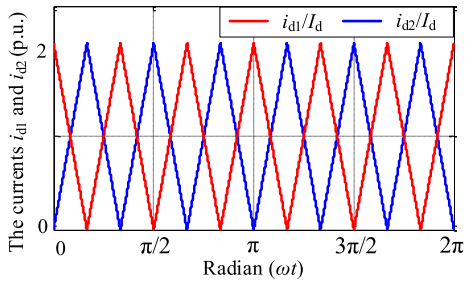

Fig. 11. Currents i_{d1} and i_{d2}.

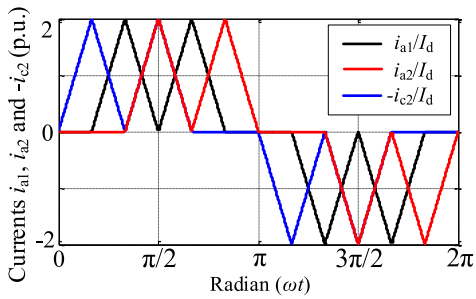

Fig. 12. Currents i_{a1}, i_{a2}, and $-i_{c2}$.

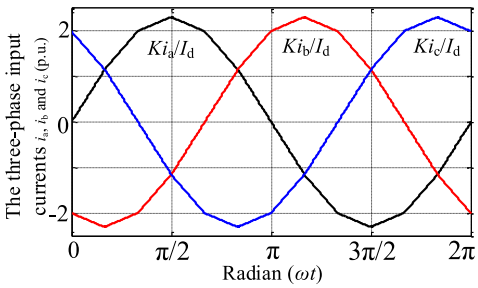

Fig. 13. Three-phase input currents.

From Fig. 12, the Fourier series of currents i_{a1}, i_{a2}, and $-i_{c2}$ are

$$\begin{cases} i_{a1} = \sum_{k=1}^{\infty} \frac{48 I_d}{(k\pi)^2} \sin(\frac{k\pi}{2})[2\cos(\frac{k\pi}{6}) \\ -\cos(\frac{k\pi}{3}) - 1] \sin k\omega t \\ i_{a2} = \sum_{k=1}^{\infty} \frac{48 I_d}{(k\pi)^2} \sin(\frac{k\pi}{2})[2\cos(\frac{k\pi}{6}) \\ -\cos(\frac{k\pi}{3}) - 1] \sin k(\omega t + \frac{\pi}{6}) \\ -i_{c2} = -\sum_{k=1}^{\infty} \frac{48 I_d}{(k\pi)^2} \sin(\frac{k\pi}{2})[2\cos(\frac{k\pi}{6}) \\ -\cos(\frac{k\pi}{3}) - 1] \sin k(\omega t + \frac{5\pi}{6}). \end{cases} \tag{34}$$

According to (22) and (34), the Fourier series of i_a in Fig. 13 can be expressed as

$$i_a = \sum_{k=1}^{\infty} \frac{48 I_d}{K(k\pi)^2} \sin\left(\frac{k\pi}{2}\right) \left[2\cos\left(\frac{k\pi}{6}\right) - \cos\left(\frac{k\pi}{3}\right) - 1\right] \cdot \left[\sin(k\omega t) - \frac{2\sqrt{3}}{3} \sin\left(\frac{k\pi}{3}\right) \cos(k\omega t + \frac{k\pi}{2})\right]. \tag{35}$$

From (35), it can be found that the (12k±1)th (k is a positive integer) harmonics are almost eliminated in the input current.

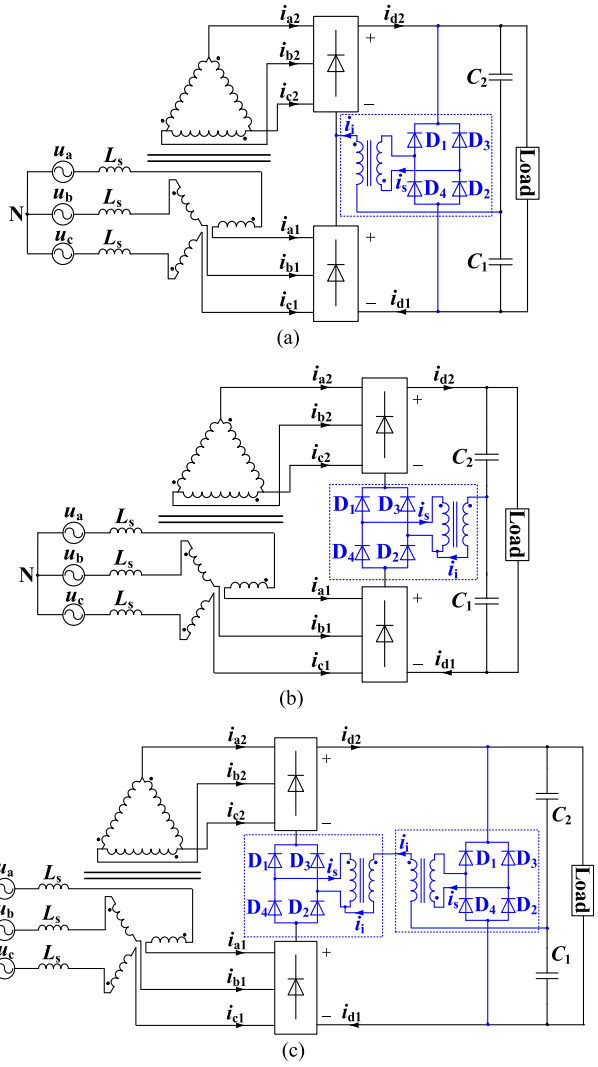

Fig. 14. Multipulse current source rectifiers based on dc side passive harmonic reduction methods. (a) 24-pulse rectifier with voltage harmonic injection circuit. (b) 24-pulse rectifier with current harmonic injection circuit. (c) 36-pulse rectifier with dual passive harmonic injection circuits.

In combination with the control and drive circuit, the basic harmonic reduction mechanism of the active HPR is providing a specific current that can modulate the input current into near-sinusoidal waves, thereby reducing the harmonic content in the input currents. The waveform and amplitude, phase, frequency information of the injection current can refer to the above analysis.

III. DC Side Passive Harmonic Reduction Methods

Fig. 14 shows three kinds of DC side HRCs for a current source rectifier [26]–[28], their HRCs are consisted with single-phase transformer and single-phase diode bridge rectifier.

The configuration and operation modes of the rectifier shown in Fig. 14(a) are similar to that of Fig. 1, so that they have same harmonic reduction mechanism. Compared with Fig. 14(a), the HRC in Fig. 14(b) has same components but with different connection method, that can provide current harmonics for the main circuit. In Fig. 14(b), the dc side of the single-phase diode bridge rectifier is connected in series with the three-phase rectifiers, and the ac side is connected with the single-phase transformer. When i_{d2} is much greater than i_{d1}, diodes D_1 and D_2 are turned ON (see mode 1); with the gradually decrease of i_{d2} and the increase of i_{d1}, when the current difference between i_{d2} and i_{d1} can be provided by the single-phase rectifier, four diodes are turned on at the same time (mode 2), this mode continues to the moment when i_{D3} is equal to i_{d2} and i_{D4} is equal to i_{d1}; so in mode 3, diodes D_3 and D_4 are turned ON; during the currents transfer from D_3 and D_4 to D_1 and D_2, there is a transition stage (mode 4) that is same with mode 2, and this mode is end when i_{D1} is equal to i_{d2} and i_{D2} is equal to i_{d1}. Based on current relations on both sides of the injection transformer, the interval length of modes 2 and 4 is associated with turns ratio design, once the turns ratio is determined, the interval length can also be determined. Although this harmonic reduction method is more complex, this connection way provides a new idea for construction of dual passive HRC.

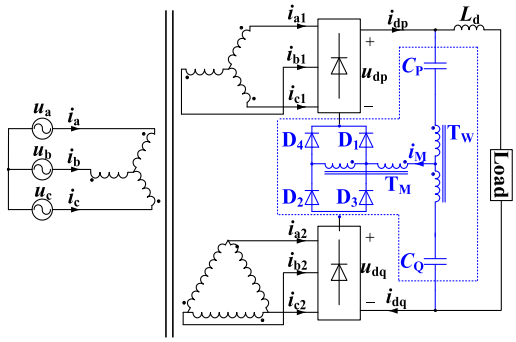

Fig. 15. 24-pulse voltage source rectifier with single-phase bridge rectifier.

As shown in Fig. 14(c), this rectifier combines HRCs in Fig. 14(a) and (b) to produce a dual passive harmonic reduction method, which can be operated in a 36-pulse rectification state. Based on the operation modes of these two kinds of passive HRC in Fig. 14(a) and (b), six operation modes of this dual passive HRC can be obtained, in combination with operation modes of three-phase rectifiers, there exist 36 combinations of all operation modes, so that the input voltage of the phase-shifting transformer has 36 steps per cycle.

Only passive devices are used in these three HRCs that are easy to implement. Moreover, harmonic reduction methods presented in Fig. 14 are all suitable for an isolated transformer, which provides another choice for some occasions need electrical isolations.

Fig. 15 is a 24-pulse voltage source rectifier with a single-phase diode bridge rectifier [29], the HRC is similar with that in Fig. 14(b), but in the voltage source rectifier, one more single-phase transformer needs to be added between two capacitors to keep balance of currents flowing into two capacitors. The conduction modes of the single-phase rectifier are determined by the voltage relations between u_{dp} and u_{dq}, due to that u_{dp} and u_{dq} are six-pulse waves with a phase difference of 30°, there are two operation modes of the single-phase bridge rectifier, and

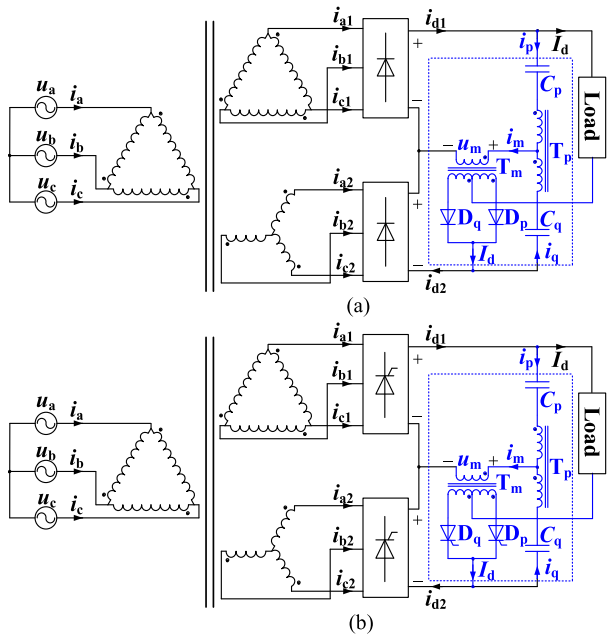

Fig. 16. 24-pulse voltage source rectifier with single-phase full-wave rectifier. (a) Diode-based 24-pulse rectifier. (b) Thyristor-based 24-pulse rectifier.

the actual direction of the current i_{M} changes as the diodes' conduction mode changes. Based on KCL, i_{dp} and i_{dq} are two sets of square waves with a phase difference of 30° at a frequency of six times power frequency, therefore, a 24-step input current can be obtained at the ac side of the rectifier. This method contains two single-phase transformers, which increases total cost and volume of the system.

Fig. 16 (a) gives another topology of the 24-pulse rectifier [30]. There are also two operation modes of the single-phase full-wave rectifier, so that same harmonic reduction effect can be obtained by using this circuit.

If the diodes in Fig. 16(a) are replaced by thyristors, the thyristor-based rectifier can be constructed [see Fig. 16(b)]. It is indicated that the harmonic reduction mechanism and optimum turns ratio of the single-phase transformer T_m in these two topologies are the same [31]. In combination with the phase angle control, the thyristor-based rectifier can also operate under 24-pulse rectification state and the RMS value of the load voltage can be changed by changing the firing angle of the thyristors.

On the basis of Fig. 16(b), the pulse number of the rectifier can be extended to $12n$ when using an n-tap transformer and n thyristors in the HRC.

From Fig. 16, the HRCs for the diode or thyristor-based rectifiers have some similarities, the HRCs suitable for the diode-based rectifiers can also be used in the thyristor-based rectifiers after changing device type. Compared with diode-based rectifiers, thyristor-based rectifiers are more suitable for some occasions that need voltage regulation, such as motor drive, high voltage direct current (HVdc) transmission, etc.

For current source rectifiers, the input current harmonics can be indirectly eliminated through increasing the step number of the input voltages; however, for voltage source rectifiers, the input current harmonics can be directly eliminated by increasing the step number of the currents. The comparisons of the above-mentioned passive HRCs are given in Table V, and their advantages and disadvantages are given in Table VI.

IV. DC Side Active Harmonic Reduction Methods

Generally, dc side active harmonic reduction methods can be divided into two kinds, which are harmonic injection methods and dc side current modulation methods. The harmonic reduction mechanism of the former method is similar to that of the passive harmonic reduction method, the harmonics in the input currents can be eliminated through increasing the step number of the input currents or voltages. By controlling the operation modes of the active HRC, the current modulation method can modulate the output currents of the three-phase rectifiers into the required shapes, so that the input currents can be modulated into sinusoidal waves.

A. Harmonic Injection Methods

Fig. 17 shows three series-connected MPRs with three kinds of DC side voltage harmonic injection circuits [32]–[34]. In Fig. 17(a), the voltage harmonic injection circuit is consisted with a single-phase transformer and a single-phase thyristor bridge rectifier. By optimizing the turns ratio of the single-phase transformer and controlling the switching states of the single-phase thyristor bridge rectifier, the winding voltage of the single-phase transformer can be modulated to a three-step wave with the frequency of $6f_{\mathrm{s}}$, thereby forming a 36-step voltage on the primary side of the isolation transformer.

Fig. 17 (b) adds one more harmonic injection circuit on the basis of Fig. 17(a). Based on a similar control method, both single-phase transformers can obtain a three-step voltage with a certain phase difference at a frequency of $6f_{\mathrm{s}}$. Therefore, a five-step voltage is injected into the dc side of the main circuit, so that the primary voltage of the isolation transformer is a 60-step wave.

Based on Fig. 17(b), Fig. 17(c) combines and simplifies two single-phase transformers and two sets of single-phase thyristor rectifier bridges to form a simplified MPR. In Fig. 17(c), the two secondary windings of the single-phase transformer are, respectively, connected to two sets of thyristor rectifier bridges. The two sets of thyristor rectifier bridges share a bridge arm, which reduces the use of thyristors, but can achieve identical harmonic reduction effects.

Fig. 18 presents three voltage source rectifiers with three kinds of dc side active current harmonic injection circuits [35]–[37]. The voltage difference of the three-phase bridge rectifiers' output voltages is provided for the single-phase thyristor rectifier through the secondary side of the single-phase transformers.

In Fig. 18(a), the harmonic injection circuit consists of two capacitors, two single-phase transformers, and a single-phase thyristor rectifier bridge. By controlling the operation modes of the single-phase thyristor rectifier bridge, the current flows in the single-phase transformer can be changed directionally, so that the winding current of the single-phase transformer is a square wave with the frequency of $6f_{\mathrm{s}}$. The square-wave currents can be

TABLE V
COMPARISONS ON THE MPRS WITH DC-SIDE PASSIVE HRCS

Fig. No.	Pulse Number	$THD_{inpt\ current}$	kVA Ratings of Magnetic Devices (% load power)	Applications
Fig. 1	24	2.65%	main transformer: over 100%; single-phase transformer: 2.3%.	high-power rectifications
Fig. 14 (a)	24	2.57%	main transformer: ~50%; single-phase transformer: ~2%.	more electric aircraft; aerospace industry.
Fig. 14 (b)	24	2.48%	main transformer: ~50%; single-phase transformer: ~1.6%.	
Fig. 14 (c)	36	1.51%	main transformer: ~50%; two single-phase transformers: together ~2%.	
Fig. 15	24	7.5% in theory	/	high-voltage & high-power occasions
Fig. 16 (a)	24	7.5% in theory	main transformer: ~109.4%; two single-phase transformers: together ~6.5%.	

TABLE VI
ADVANTAGES AND DISADVANTAGES FOR MPRS WITH DC-SIDE PASSIVE HRCS

Fig. No.	Advantages	Disadvantages
/	***For all series-connected MPRs***: avoid current unbalance between two series-connected three-phase rectifiers; ***For all diode MPRs with passive harmonic reduction circuit***: high reliability, easy to realize, economic and efficient; ***For all current-source series-connected MPRs with DC side filter capacitors*:** load u/i ripple factor is quite low.	limited harmonic reduction ability
Fig. 1	can provide galvanic isolation	lower power density
Fig. 14	reduced kVA rating of the main transformer	cannot provide galvanic isolation
Fig. 15	eliminated phase difference between input current and voltage source; high power factor.	need additional single-phase transformer; power quality on both AC and DC sides are reduced compared to current source MPRs.
Fig. 16	change diodes into N thyristors can form $12N$-pulse rectifiers	

injected into the three-phase rectifier bridges by the single-phase transformers, finally, the ac side input current is changed from a 12-step wave to a 24-step wave.

The HRC in Fig. 18(b) adds a bypass thyristor connected in parallel at both ends of the single-phase thyristor rectifier bridge. By controlling the ON and OFF states of five thyristors, the winding current of the single-phase transformer is changed into a three-step wave, which is also injected into the three-phase rectifier bridge through single-phase transformers, and finally the AC-side input current is changed to a 36-step wave.

Based on Fig. 18(a) and 18(b), by increasing the number of single-phase transformer secondary windings and single-phase thyristor rectifier bridges in the harmonic injection circuit, an input current of any number steps can be obtained as shown in Fig. 18(c). The number of secondary windings and single-phase thyristor rectifier bridges is proportional to the step number of the injected current. According to the level of the injected dc side current, MPRs with different pulse number can be constructed. However, with the increase in the number of secondary windings and single-phase thyristor rectifier bridges, the size and cost of the system will also increase, and switching losses will inevitably increase. At the same time, the increase in the number of thyristors means that the complexity of control methods also increases.

From Figs. 17 and 18, the dc-side harmonic injection circuit is generally composed of thyristors, single-phase transformers, and capacitors. Its harmonic suppression capability is directly proportional to the number of thyristors. The rectifier can obtain better harmonic suppression performance, but the complexity of the control circuit will inevitably increase.

B. Current Modulation Methods

The rectifier shown in Fig. 19 is a current source rectifier whose ac side inductors can be omitted because they are folded into transformer inductances [38]. Its current modulation circuit consists of a single-phase transformer and a single-phase inverter. The dc side of the single-phase inverter is connected across the output capacitor, and its ac side outputs a square wave voltage with a variable amplitude and a frequency of $6f_s$. The output currents of the two sets of rectifier bridges can be modulated into a triangular wave at frequency of $6f_s$ with the same average value and opposite phases, which can ultimately reduce the THD of the ac side input current to around 3.57%. The capacity of the current modulation circuit is only 4.8% of the load power, and the harmonic suppression cost is small. Compared with Fig. 14 (a), in Fig. 19, the use of active devices cannot increase the step number of the injected voltage, so that the harmonic reduction effect has not been significantly improved. However, different

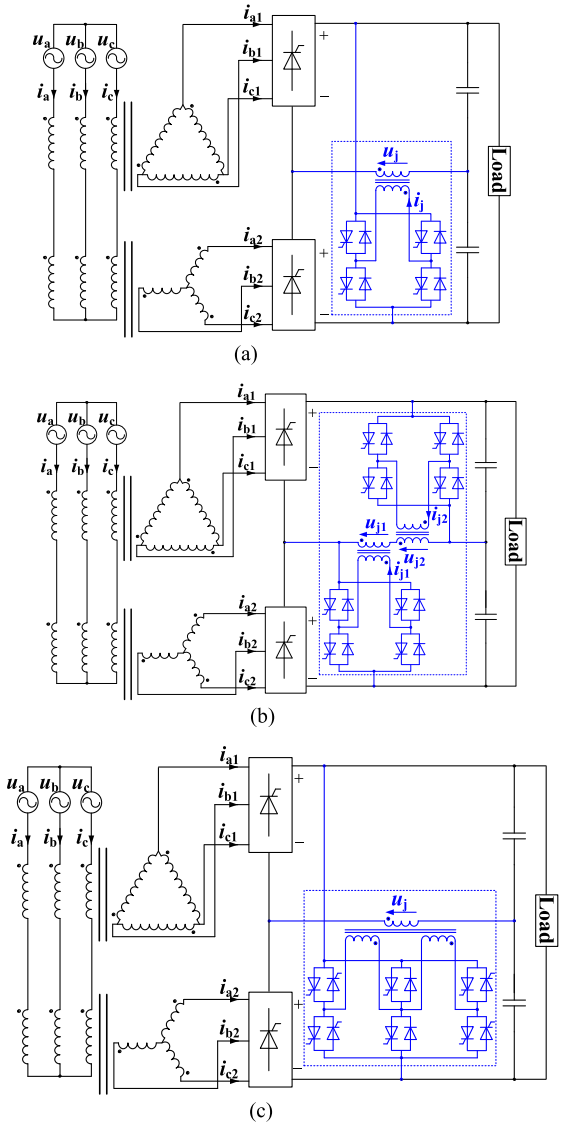

Fig. 17. Multipulse current source rectifiers with harmonic injection circuits. (a) 36-pulse rectifier with single-phase thyristor bridge rectifier. (b) 60-pulse rectifier with two single-phase thyristor bridge rectifiers. (c) 60-pulse rectifier with simplified thyristor bridge rectifier.

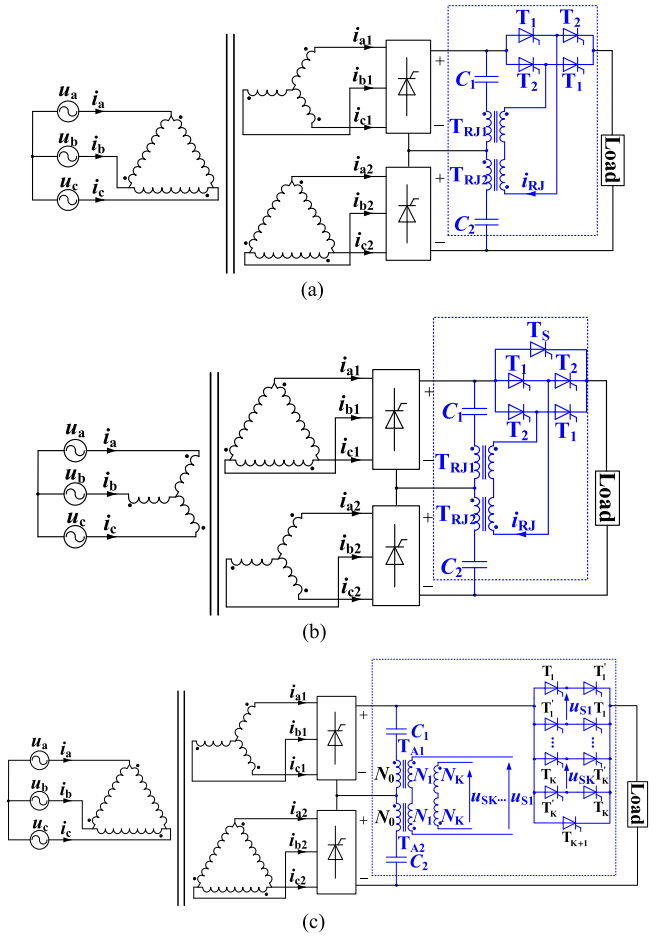

Fig. 18. Multipulse voltage source rectifiers with harmonic injection circuits. (a) 24-pulse rectifier with single-phase thyristor bridge rectifier. (b) 36-pulse rectifier with bypass thyristor bridge rectifier. (c) MPR with single-phase thyristor bridge rectifiers.

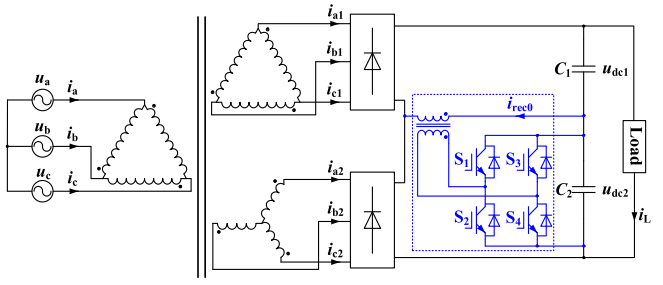

Fig. 19. Series-connected MPR with single-phase inverter.

from the passive method, the control circuit used in Fig. 19 has the function of eliminating the phase difference between the three-phase voltage sources and the input currents of the rectifier, which can improve the power factor of the rectifier.

Fig. 20 shows a series MPR with a single-phase half-bridge PWM inverter [39]. This rectifier adds a PWM inverter to the dc side of the series 12-pulse rectifier. The control circuit corrects control signals of insulated-gate bipolar transistors (IGBTs) through a current-mode hysteresis comparator, thus the output currents of the three-phase bridge rectifiers are modulated into triangular waves with a phase difference of 30° at a frequency of $6f_s$ so that the waveform of the input current on the ac side is approximately a sine wave. When the auxiliary circuit fails, the rectifier can be operated in 12-pulse rectification state. Compared with the conventional PWM rectifier, this method reduces the cost, and the capacity of the current modulation circuit only accounts for a small part of the output power. However, because the control signals of the two IGBTs are received by the hysteresis comparator, the output current of the rectifier bridge has some obvious ripples.

Fig. 21 shows a series MPR with dc side buffer circuit [40]. The output terminals of the two sets of three-phase rectifier bridges are connected in series with the IGBTs. By controlling the ON and OFF states of the IGBTs, the output currents of the

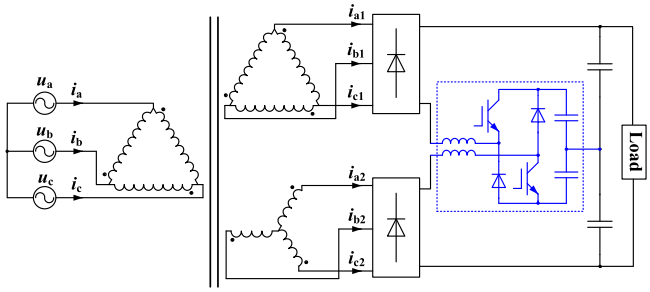

Fig. 20. Series-connected MPR with PWM converter.

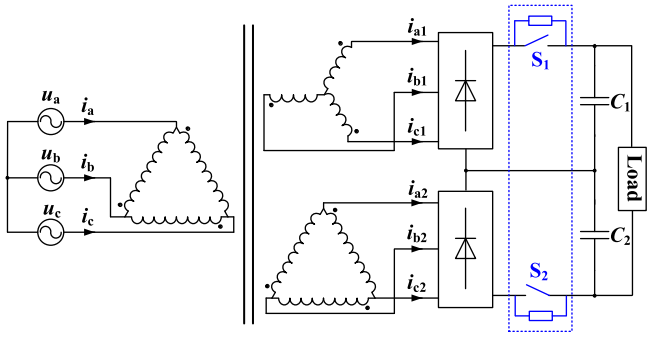

Fig. 21. Series-connected MPR with buffer circuit.

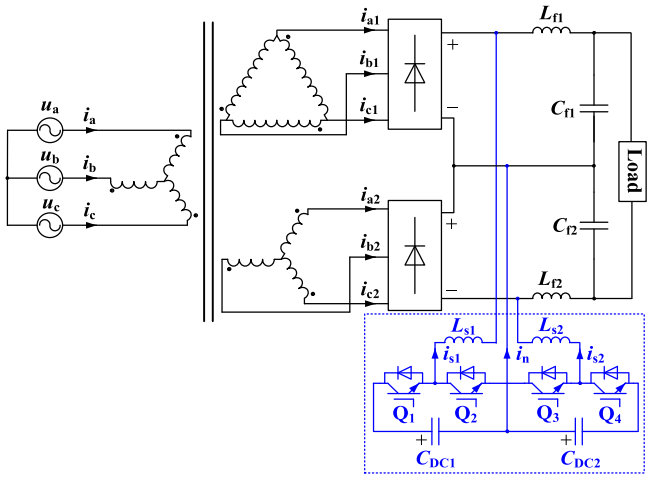

Fig. 22. Series-connected MPR with buck-boost converter.

three-phase bridge rectifiers can be modulated into triangular waves so that the input current on the ac side is approximately a sine wave with a THD value of 1.37%. This method can effectively reduce the harmonic content of the input current when the load changes rapidly, and when the IGBT fails to commutate, the rectifier can be temporarily operated in the 12-pulse rectification state by shorting the IGBTs, so it is convenient for fault handling. However, the buffer circuit is directly connected in series with the main circuit, which may result in large switching losses.

In Fig. 22, the current modulation circuit consists of a cascaded buck-boost converter [41]. The cascaded buck-boost converter can modulate the output current of the three-phase rectifier

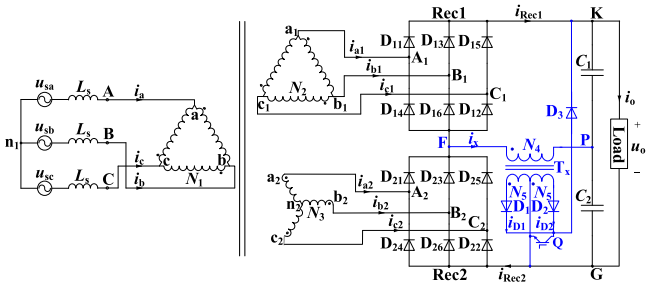

Fig. 23. Series-connected 36-pulse rectifier with hybrid HRC (full-isolated phase-shifting transformer).

bridge into triangular waves, thereby reducing the harmonic content of the input current of the rectifier, making its THD value only 2.41%. This method can provide an energy transmission interface for the system that can be used to transmit active power into the dc bus. When the bridge rectifiers are operating under discontinuous conduction mode, the method still has good harmonic suppression ability. The drawback of this method is that the control circuit is more complicated and the switching loss is larger.

Although the current modulation methods shown in Figs. 17 to 22 all have considerable harmonic suppression effect, but may have disadvantages of large switching losses or complex control circuit design. Their power quality comparisons, suitable occasions, advantages and disadvantages are given in Table VII.

V. DC Side Hybrid Harmonic Reduction Methods

According to the current research status of dc side passive and active harmonic reduction methods, although the passive harmonic reduction method has a simple structure and low implementation difficulty, the harmonic reduction effect is limited. Some active methods can improve the harmonic reduction ability, but have disadvantages of complex control circuits and large switching losses. Therefore, a combination of passive and active harmonic reduction methods is considered to form a dc-side hybrid harmonic reduction method.

Fig. 23 is a series-connected 36-pulse rectifier with dc side hybrid HRC [42], this circuit is designed based on the passive HRC presented in Fig. 1, one more switch and a diode is added into the original passive HRC. The output currents of the two three-phase rectifiers are still six-pulse waveforms, so that the current difference is a triangular wave with a frequency of $6f_s$. When taking the zero-crossing moment of the triangle wave current as the center point to design conduction angle of the bidirectional switch, a three-step wave can be generated on the primary side of the single-phase transformer. Finally, a 36-step input voltage is obtained. The THD value of the input current reduces to $\sim$2% in experiment.

Fig. 24 is a series-connected 36-pulse rectifier with dc side hybrid HRC which is constructed based on the passive HRC shown in Fig. 14 [43]. A new-added bidirectional switch is connected in parallel with the primary side of the harmonic injection transformer. After using this method, the THD value of the AC side input current reduces to 1.2%, the capacity of the

TABLE VII
COMPARISONS ON THE MPRS WITH DC-SIDE ACTIVE HRCS

Fig. No.	Pulse Number	THD	Applications	Advantages	Disadvantages
Fig. 17 (a)	36	5.09% (*u*)	high voltage occasions	switching frequencies for the main circuit and HRC are f_s and $6f_s$; total switching losses are quite low.	control circuit is more complex with increases of pulse number
Fig. 17 (b)	60	3.16% (*u*) 0.09% (*i*)			
Fig. 17 (c)	60	1% (*u*)			
Fig. 18 (a)	24	/	HVDC systems	easy to expand to more pulse number	need two sets of single-phase transformers; load ripple factor is higher than current source rectifiers; control circuit is more complex with increases of pulse number.
Fig. 18 (b)	36	/			
Fig. 18 (c)	multi-pulse	/			
Fig. 19	24	3.57% (*i*)	aluminum refining, traction substation, and AC drive.	phase difference of the input currents and voltage sources can be eliminated; can degrade to 12-pulse rectifier when the HRC is fault.	the carrier frequency is 10kHz and switching power losses is high
Fig. 20	/	near to sinewaves	HVDC systems	almost eliminate all harmonics; lower voltage rating of the DC side PWM modulator; no requirement for additional single-phase transformer.	may cause high switching power losses
Fig. 21	/	0.84% (*i*)		achieve unity power factor; high-quality current/voltage at both sides of the rectifier.	
Fig. 22	/	2.41% (*i*)	high-power industry, vehicle charging stations, more electric ships and aircrafts.	no requirement for additional single-phase transformer; can provide energy storage interface to the system.	high complexity of control circuit design

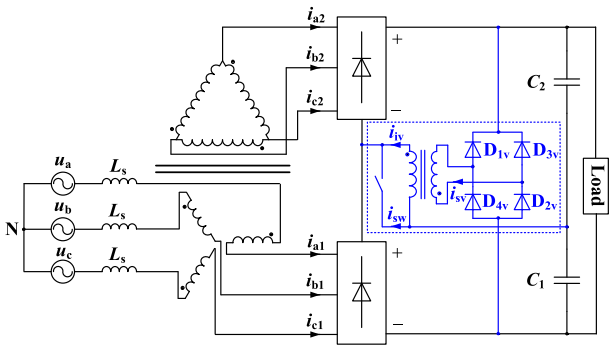

Fig. 24. 36-pulse current source rectifier with hybrid HRC (half-isolated phase-shifting transformer).

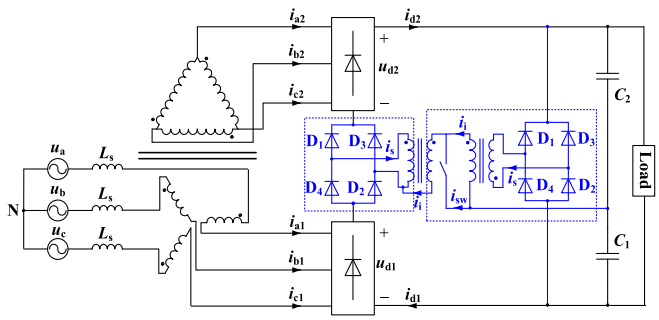

Fig. 25. 48-pulse current source rectifier with hybrid HRC.

single-phase transformer is only 1.9% of the load power, and the RMS value of the current flowing through the bidirectional switch is only 1.5% of the load current, so that the harmonic injection circuit only accounts for a small part of the load power.

Fig. 25 is a 48-pulse rectifier with dc side hybrid HRC which combines the active bidirectional switch with the dual passive harmonic reduction method [44]. As mentioned before, there are six operation modes of the dual passive HRC per cycle, in order to keep the cycle-symmetry, two modes when switch is turned on are added into the original six modes. Therefore,

TABLE VIII
COMPARISONS ON THE MPRS WITH DC-SIDE HYBRID HRCS

Fig. No.	Pulse Number	THD	Applications	Advantages	Disadvantages
Fig. 23	36	3.29%(u) 2%(i)	high-power rectifications	only use one switch, lower switching losses, easy control, can provide galvanic isolation.	requires control and drive circuitry with sensing devices to synchronize the operation of the switch
Fig. 24	36	1.2%(i)	DC railway system, HVDC transmission.	the frequency of the switch operates at $6f_s$ and have a low rating	
Fig. 25	48	3.74%(u)	more electric aircraft	lower kVA ratings of additional single-phase transformers which are 0.5% and 1.4% of load power	
Fig. 26	/	2.36% for 24-pulse operation and 1.06% for PWM operation	HVDC transmission, aircraft systems.	do not use injection transformer; can provide high quality input currents.	high power losses in PWM operation mode

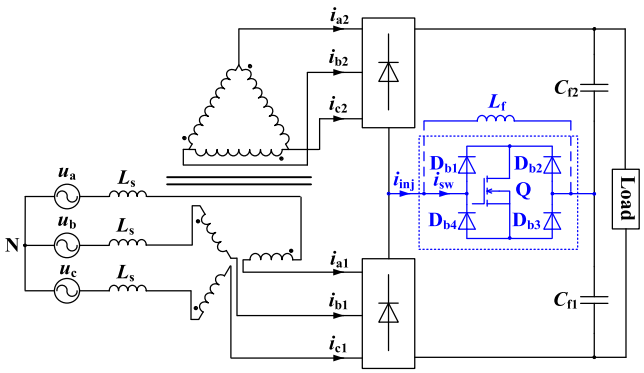

Fig. 26. Multipulse current source rectifier with hybrid HRC.

there are eight operation modes of the hybrid HRC. The switch conduction angle is still centered on the zero-crossing point of the current difference. The level number of the voltage u_{d1} and u_{d2} is changed from four to five, which contributes to the formation of the 48-step input voltage. The overall VA-rating of the two harmonic injection transformers is 1.9% of the load power and the RMS value of the current flowing through the switch is only 1% of the load current.

Fig. 26 shows a series MPR with a hybrid harmonic injection circuit [45]. This hybrid HRC is composed of four diodes and a switching tube, which can be equivalent to a bidirectional switch. When the driving signal of the switch is a pulse signal at a frequency of $12f_s$ and with a duty cycle of 0.5, the rectifier works in the 24-pulse rectification state. When the driving signal of the switch is a high-frequency pulse signal with pulse width modulation, the rectifier works in the multilevel PWM rectification state, and the THD value of the input current is decreased to 1.06%. This method uses a bidirectional switch instead of a single-phase injection transformer, which reduces the weight and volume of the system to a certain extent.

Table VIII gives the power quality, suitable occasions, advantages and disadvantages of the hybrid harmonic reduction methods in this section.

VI. SIMULATION VERIFICATIONS

In this section, some simulation results are presented to verify harmonic reduction mechanisms and compare properties of some aforementioned topologies. All simulation models established in this part are used $\Delta/\Delta/Y$ isolated transformer with turns ratio of $3\sqrt{3}{:}\sqrt{3}{:}\ 1$; the RMS values of the three-phase voltage sources are 220V; the filter inductors are 20 mH; the dc side capacitors are 3300 μF; load type of current source MPRs is resistive load (60 Ω), and load type of voltage source MPR is *R–L* load (100 mH, 60 Ω); all simulation results are obtained under optimum turns ratio and conductive angle design.

Table IX gives harmonic contents in input voltages and input currents of the current source 12-, 24- and 36-pulse MPRs. Figs. 27 and 28 are simulation results of current and voltage source 24-pulse rectifiers with dc side passive HRCs, respectively. Fig. 29 presents simulation results of the 12-pulse rectifier with dc side active HRC. Besides, to do comparisons, Fig. 30 are results of the 36-pulse rectifier with hybrid HRC. Based on the above simulation results, it can be obtained that the following.

1) For the MPRs with dc side passive/hybrid HRCs, the main current/voltage harmonics in the *N*-pulse rectifier are ($Nk\pm1$)th, k is a positive integer. The THD value decreases with the increasing of the pulse number, and the harmonic content decreases with the increase of the harmonic order. For the voltage source *N*-pulse rectifier, the input voltages are pure sine waves and the input currents have *N* steps. For the current source *N*-pulse rectifier, the input voltage of the phase-shifting transformer has *N* steps, the harmonic orders in input currents are consistent with that in input voltages, their variation trends are also maintaining synchronization. Using passive HRC or combining switches with passive HRC are useful for improving ac side power

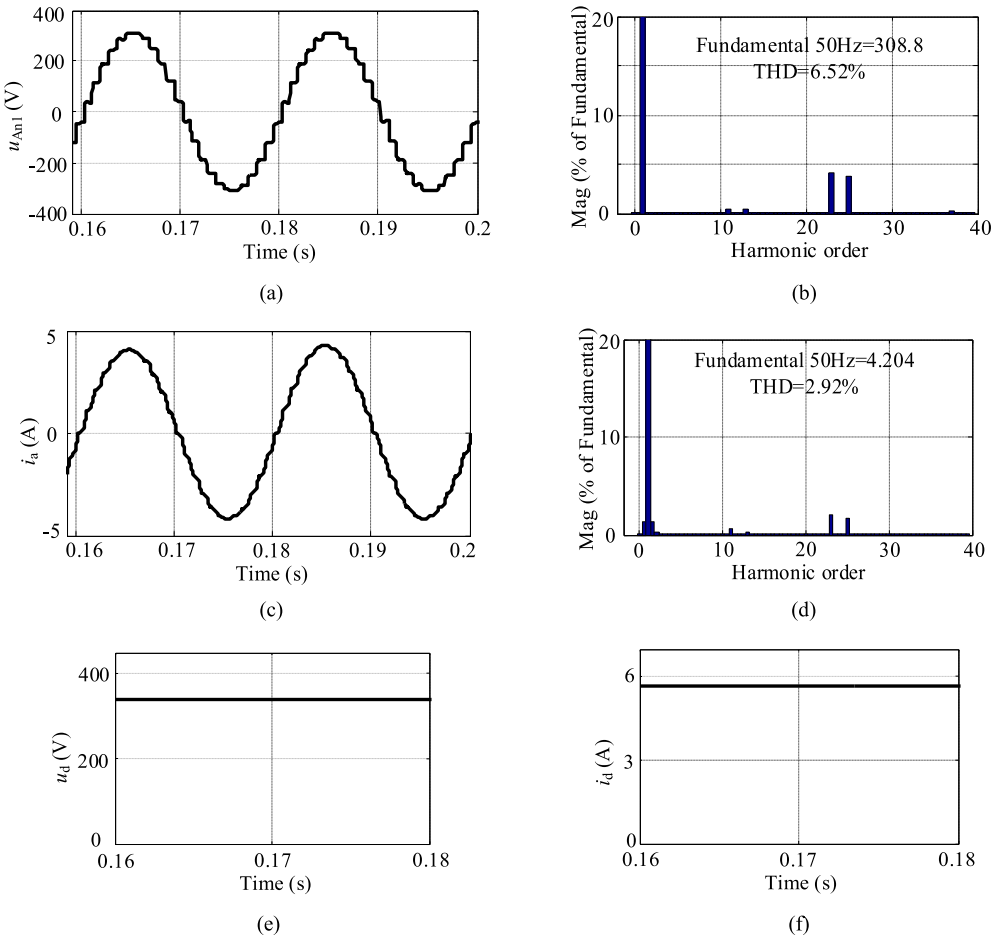

Fig. 27. Simulation results of the current source 24-pulse rectifier shown in Fig. 1. (a) Input voltage u_{An1}. (b) Spectrum of the input voltage u_{An1}. (c) Input current i_a. (d) Spectrum of the input current i_a. (e) Load voltage u_d. (f) Load current i_d.

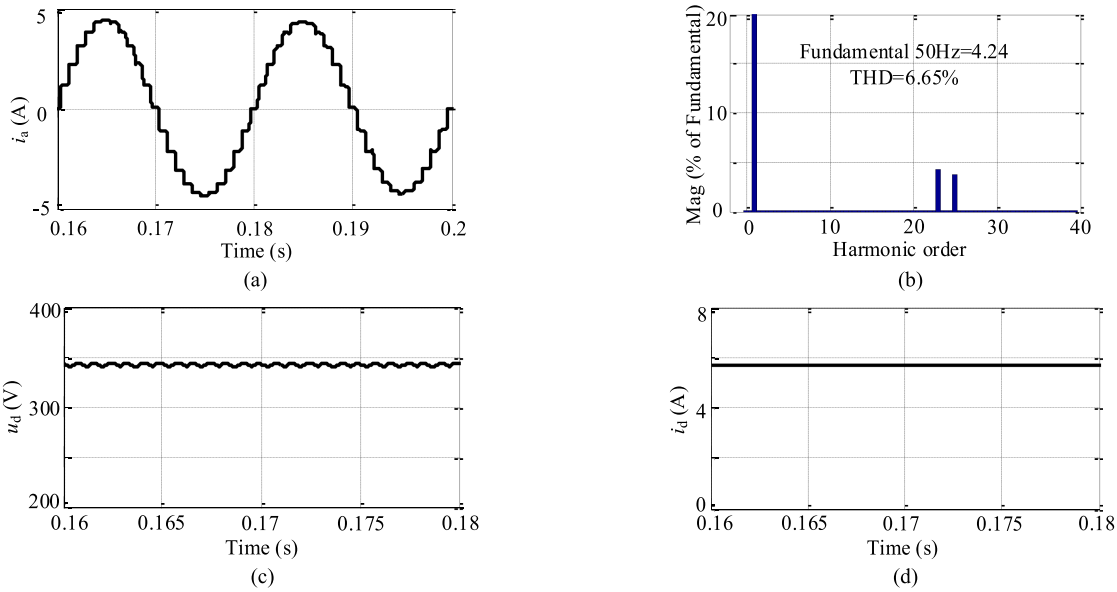

Fig. 28. Simulation results of the voltage source 24-pulse rectifier shown in Fig. 16. (a) Input current i_a. (b) Spectrum of the input current i_a. (c) Load voltage u_d. (d) Load current i_d.

TABLE IX
HARMONIC CONTENTS OF CURRENT SOURCE MPRS

Pulse Number	Figure Number	Harmonic Contents (1st=100%)								THD
		u/*i*	11th	13th	23rd	25th	35th	37th	47th	49th	
12	/	u_{An1}	7.1%	5.30%	2.16%	2.12%	1.81%	1.69%	1.13%	1.08%	10.26%
		i_a	7.21%	4.55%	1.05%	0.95%	0.58%	0.51%	0.27%	0.25%	8.69%
24	Fig. 1	u_{An1}	0.51%	0.36%	4.12%	3.74%	0.17%	0.18%	1.71%	1.60%	6.52%
		i_a	0.54%	0.33%	2.11%	1.76%	0.06%	0.06%	0.43%	0.38%	2.92%
36	Fig. 23	u_{An1}	0.43%	0.96%	0.29%	0.70%	1.40%	1.21%	0.37%	0.47%	2.87%
		i_a	0.46%	0.87%	0.15%	0.32%	0.47%	0.38%	0.09%	0.11%	1.25%

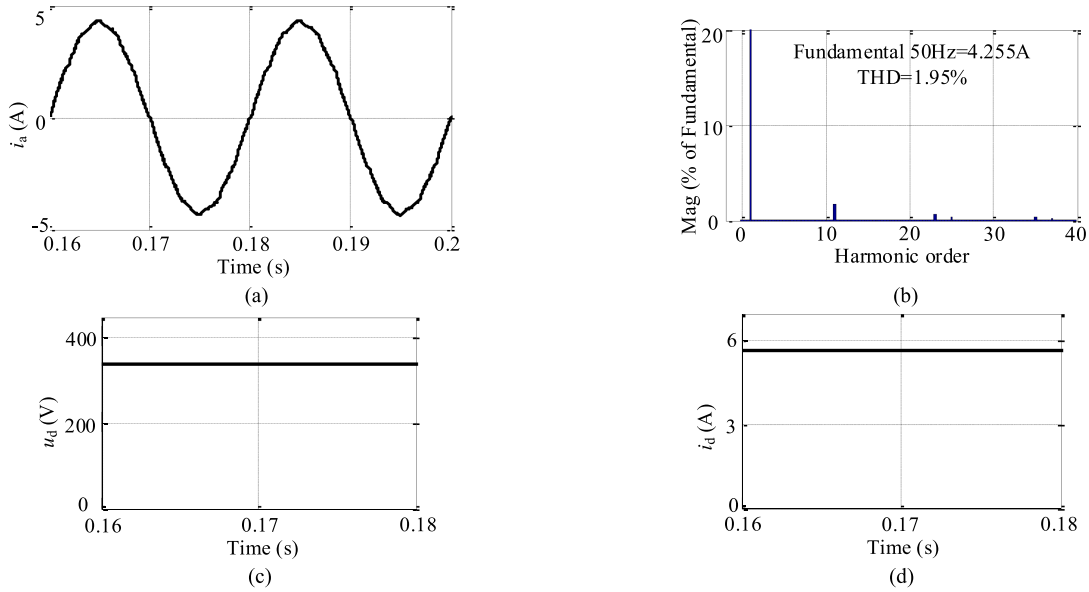

Fig. 29. Simulation results of the current source 12-pulse rectifier shown in Fig. 19. (a) Input current i_a. (b) Spectrum of the input current i_a. (c) Load voltage u_d. (d) Load current i_d.

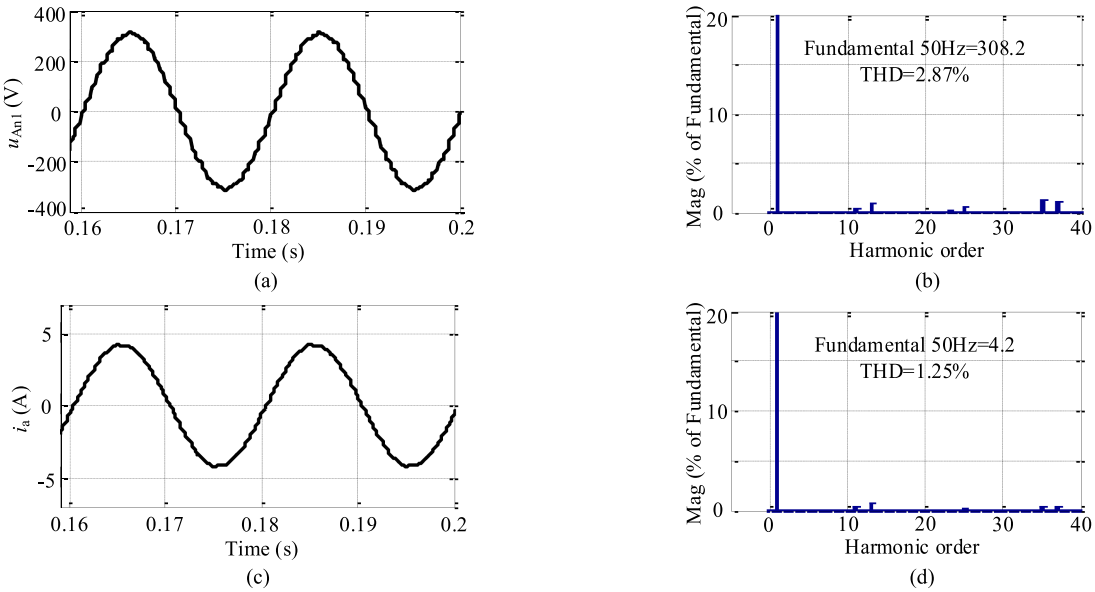

Fig. 30. Simulation results of the current source 36-pulse rectifier shown in Fig. 23. (a) Input voltage u_{An1}. (b) Spectrum of the input voltage u_{An1}. (c) Input current i_a. (d) Spectrum of the input current i_a.

quality, the input current THD value can be reduced to 1.25% after using hybrid HRC.

2) For the 12-pulse rectifier with dc side active HRC, the phase difference caused by the ac filtering inductors is eliminated, the input current is close to sinusoidal waves with the THD value of $\sim$1.95%.
3) For current source MPRs, due to the filter effect of the dc side capacitors, the load voltage can be seen as a constant value; under resistive load conditions, the load current is also constant. Therefore, they are suitable for occasions with high power quality requirements. For the voltage source 24-pulse rectifier, under large inductive load conditions, the load current is constant; however, the load voltage has 24 pulses per power cycle and the ripple coefficient is higher, which has properties just as a parallel-connected rectifier.

In addition to the linear load, MPRs are often connected to nonlinear load in practical applications, such as dc/dc or dc/ac converters.

For the voltage source rectifier, an *LC* filter must be added between the MPR and the dc/dc or dc/ac converter. Based on the operation modes of the circuit and the expected filtering effect, the proper *LC* parameter can be determined. Under the appropriate *LC* parameter setting, the power quality of the ac side input current can be kept in an ideal state. Similarly, for the current source rectifier, the value of dc filter capacitor is one of the most important parameters that affect the power quality of the MPR under load changes. Combining the operation mode and load parameters, the value range of the capacitor can be determined, and the power quality of the MPR can be controlled in an ideal state under the appropriate capacitor value.

VII. Conclusion

This article is focused on dc side harmonic reduction mechanism research and useful harmonic reduction method comparisons on the series-connected MPRs. The main contributions of this article are concluded as follows.

1) The operation modes of the series-connected 12-pulse rectifier before and after using dc side passive/active harmonic reduction methods are detailed presented in this article, from pulse number increasing and current modulating processes, mechanisms of passive/active harmonic reduction methods are determined, which are foundations for understanding and constructing novel MPRs.
2) Many useful dc link HRCs are investigated and compared in this article from viewpoint of harmonic reduction ability, complexity of implement, suitable occasions, efficiency and reliability; their operation principles, corresponding advantages and disadvantages are comprehensively clarified. This article has not been done in previous papers.
3) Based on some specific topologies, the simulation models have been built to verify the reasonability of the HRC design. From the verification results, the characteristics of each kind of harmonic reduction methods are confirmed and concluded.

Each harmonic reduction method has its own advantages and drawbacks, when doing choices or designing novel topologies, on the premise of meeting power quality requirements, a reasonable tradeoff should be considered between circuit properties and design complexity of MPRs. All above works are expected to provide useful guidelines for designers and researchers to select or design suitable MPRs under needed occasions with optimum characteristic.

With oriented of harmonic reduction mechanisms, and based on previous dc side HRCs, the development trends of MPRs design will towards higher power quality, power density, efficiency and reliability, lower complexity and losses. Considering that the current source rectifiers can provide high power quality on both ac and dc sides, the novel series-connected MPR design should pay more attention to the current source rectifiers. Currently, most of the proposed series-connected MPRs take the isolated or half-isolated transformer as the phase-shifting transformer, in future research, autotransformer design for the series-connected MPRs should become one of the key points that helps to improve the power density. Compared with active or hybrid harmonic reduction methods, the passive harmonic reduction methods are much easier to realize. If passive HRCs are combined with a basic topology with higher pulse number, better ac side power quality can be obtained. Moreover, the fault tolerance and novel control methods research should also be done in future. These researches are useful for improving the overall performance of MPRs.

References

[1] Q. Du, L. Gao, Q. Li, T. Li, and F. Meng, "Harmonic reduction methods at DC side of parallel-connected multipulse rectifiers: A review," *IEEE Trans. Power Electron.*, vol. 36, no. 3, pp. 2768–2782, Mar. 2021.

[2] D. A. Paice, *Power Electronics Converter Harmonics: Multipulse Methods For Clean Power*. Hoboken, NJ, USA: Wiley, Sep. 1999.

[3] S. Kwak and H. A. Toliyat, "Current-source-rectifier topologies for sinusoidal supply current: Theoretical studies and analyses," *IEEE Trans. Ind. Electron.*, vol. 53, no. 3, pp. 984–987, Jun. 2006.

[4] J. Chen, Y. Shen, J. Chen, H. Bai, C. Gong, and F. Wang, "Evaluation on the autoconfigured multipulse AC/DC rectifiers and their application in more electric aircrafts," *IEEE Trans. Transp. Electrific.*, vol. 6, no. 4, pp. 1721–1739, Dec. 2020.

[5] J. R. Rodríguez *et al.*, "Large current rectifiers: State of the art and future trends," *IEEE Trans. Ind. Electron.*, vol. 52, no. 3, pp. 738–746, Jun. 2005.

[6] A. Xu and S. Xie, "A multipulse-structure-based bidirectional PWM converter for high-power applications," *IEEE Trans. Power Electron.*, vol. 24, no. 5, pp. 1233–1242, May 2009.

[7] B. Singh, S. Gairola, B. N. Singh, A. Chandra, and K. Al-Haddad, "Multipulse AC-DC converters for improving power quality: A review," *IEEE Trans. Power Electron.*, vol. 23, no. 1, pp. 260–281, Jan. 2008.

[8] C. Young, M. Chen, C. Lai, and D. Shih, "A novel active interphase transformer scheme to achieve three-phase line current balance for 24-pulse converter," *IEEE Trans. Power Electron.*, vol. 27, no. 4, pp. 1719–1731, Apr. 2012.

[9] F. Meng, W. Yang, S. Yang, and L. Gao, "Active harmonic reduction for 12-pulse diode bridge rectifier at DC side with two-stage auxiliary circuit," *IEEE Trans. Ind. Inf.*, vol. 11, no. 1, pp. 64–73, Feb. 2015.

[10] Y. Lian, S. Yang, K. Xu, Y. Li, and W. Yang, "Harmonic reduction mechanism at DC link of two different 24-pulse rectifiers," in *Proc. IEEE Transp. Electrific. Conf. Expo Asia-Pac.*, 2017, pp. 1–7.

[11] Y. Li, K. Xu, Y. Lian, W. Yang, and S. Yang, "A novel 36-pulse rectifier with a low loss interphase converter at DC side," in *Proc. IEEE Transp. Electrific. Conf. Expo Asia-Pac.*, 2017, pp. 1–7.

[12] Z. Liu, F. Meng, and W. Yang, "Harmonic reduction technology at DC link in star-connected-autotransformer-based multi-pulse rectifier," in *Proc. IEEE Transp. Electrific. Conf. Expo Asia-Pac.*, 2017, pp. 1–7.
[13] F. Meng, X. Xu, L. Gao, Z. Man, and X. Cai, "Dual passive harmonic reduction at DC link of the double-star uncontrolled rectifier," *Trans. Ind. Electron.*, vol. 66, no. 4, pp. 3303–3309, Apr. 2017.
[14] F. Meng, X. Xu, L. Gao, and C. Cai, "Active harmonic reduction using DC-side current injection applied in a novel large current rectifier based on fork-connected autotransformer," *IEEE Trans. Ind. Electron.*, vol. 64, no. 7, pp. 5250–5264, Jul. 2017.
[15] F. Meng, X. Xu, and L. Gao, "A simple harmonic reduction method in multipulse rectifier using passive devices," *IEEE Trans. Ind. Informat.*, vol. 13, no. 5, pp. 2680–2692, Oct. 2017.
[16] V. Sheelvant, R. Kalpana, and B. Singh, "Improvement in harmonic reduction of zigzag autoconnected transformer based 12-pulse diode bridge rectifier by current injection at DC side," *IEEE Trans. Ind. Appl.*, vol. 53, no. 6, pp. 3634–3644, Nov./Dec. 2017.
[17] R. Kalpana, K. S. Chethana, S. Prakash P., and B. Singh, "Power quality enhancement using current injection technique in a zigzag configured autotransformer-based 12-pulse rectifier," *IEEE Trans. Ind. Appl.*, vol. 54, no. 5, pp. 5267–5277, Sep./Oct. 2018.
[18] L. Gao, X. Xu, Z. Man, and J. Lee, "A 36-pulse diode-bridge rectifier using dual passive harmonic reduction methods at DC link," *IEEE Trans. Power Electron.*, vol. 34, no. 2, pp. 1216–1226, Feb. 2019.
[19] Y. Lian, S. Yang, and W. Yang, "Optimum design of 48-pulse rectifier using unconventional interphase reactor," *IEEE Access*, vol. 7, pp. 61240–61250, Mar. 2019.
[20] F. Meng, X. Xu, L. Gao, Z. Man, and X. Cai, "Dual passive harmonic reduction at DC link of the double-star uncontrolled rectifier," *IEEE Trans. Ind. Electron.*, vol. 66, no. 4, pp. 3303–3309, Apr. 2019.
[21] B. Singh and P. Kant, "A 40-pulse multiphase staggering modular transformer with power quality improvement in multilevel inverter fed medium-voltage induction motor drives," *IEEE Trans. Ind. Appl.*, vol. 55, no. 6, pp. 7822–7832, Nov./Dec. 2019.
[22] P. Saravana Prakash, R. Kalpana, K. S. Chethana, and B. Singh, "A 36-pulse AC–DC converter with DC-side tapped interphase bridge rectifier for power quality improvement," *IEEE Trans. Ind. Appl.*, vol. 57, no. 1, pp. 549–558, Jan./Feb. 2021.
[23] B. Singh and S. Gairola, "A 40-pulse AC-DC converter fed vector-controlled induction motor drive," *IEEE Trans. Energy Convers.*, vol. 23, no. 2, pp. 403–411, Jun. 2008.
[24] R. Abdollahi and G. B. Gharehpetian, "Inclusive design and implementation of novel 40-pulse AC–DC converter for retrofit applications and harmonic mitigation," *IEEE Trans. Ind. Electron.*, vol. 63, no. 2, pp. 667–677, Feb. 2016.
[25] F. Meng, Q. Du, L. Wang, L. Gao, and Z. Man, "A series-connected 24-pulse rectifier using passive voltage harmonic injection method at DC-link," *IEEE Trans. Power Electron.*, vol. 34, no. 9, pp. 8503–8512, Sep. 2019.
[26] F. J. Chivite-Zabalza and A. J. Forsyth, "A simple, passive 24-pulse AC-DC converter with inherent load balancing using harmonic voltage injection," in *Proc. IEEE 36th Power Electron. Specialists Conf.*, 2005, pp. 76–82.
[27] F. J. Chivite-Zabalza, A. J. Forsyth, and D. R. Trainer, "A simple, passive 24-pulse AC–DC converter with inherent load balancing," *IEEE Trans. Power Electron.*, vol. 21, no. 2, pp. 430–439, Mar. 2006.
[28] F. J. Chivite-Zabalza and A. J. Forsyth, "A passive 36-pulse AC–DC converter with inherent load balancing using combined harmonic voltage and current injection," *IEEE Trans. Power Electron.*, vol. 22, no. 3, pp. 1027–1035, May 2007.
[29] Y. Nishida and M. Nakaoka, "A new harmonic reducing three-phase diode rectifier for high voltage and high power applications," in *Proc. IEEE Ind. Appl. Conf. 32nd IAS Annu. Meeting*, 1997, pp. 1624–1632.
[30] S. Choi, J. Oh, K. Kim, and J. Cho, "A new 24-pulse diode rectifier for high voltage and high power applications," in *Proc. 30th Annu. IEEE Power Electron. Specialists Conf.*, 1999, pp. 169–174.
[31] S. Choi, J. Oh, and J. Cho, "Multi-pulse converters for high voltage and high power applications," in *Proc. 3rd Int. Power Electron. Motion Control Conf.*, 2000, pp. 1019–1024.
[32] Y. H. Liu, J. Arrillaga, and N. R. Watson, "A new high-pulse voltage-sourced converter for HVDC transmission," *IEEE Trans. Power Del.*, vol. 18, no. 4, pp. 1388–1393, Oct. 2003.
[33] L. B. Perera, Y. H. Liu, J. Arrillaga, and N. R. Watson, "A five-level reinjection scheme for high pulse-voltage source conversion," *IEE Proc.-Elect. Power Appl.*, vol. 152, no. 2, pp. 209–216, Mar. 2005.
[34] Y. H. Liu, N. R. Watson, and J. Arrillaga, "A new concept for the control of the harmonic content of voltage source converters," in *Proc. 5th Int. Conf. Power Electron. Drive Syst.*, 2003, pp. 793–798.
[35] J. Arrillaga and M. Villablanca, "24-pulse HVDC conversion," *IEE Proc. C-Gener., Transmiss. Distrib.*, vol. 138, no. 1, pp. 57–64, Jan. 1991.
[36] J. Arrillaga, R. D. Brough, and R. M. Duke, "Naturally commutated thyristor-controlled high-pulse VAr compensator," *IEE Proc. Gener. Transmiss. Distrib.*, vol. 142, no. 2, pp. 219–224, Mar. 1995.
[37] M. Villablanca, M. Arias, and C. Acevedo, "High-pulse series converters for HVDC systems," *IEEE Trans. Power Del.*, vol. 16, no. 4, pp. 766–774, Oct. 2001.
[38] S. Fukuda, M. Ohta, and Y. Iwaji, "An auxiliary-supply-assisted harmonic reduction scheme for 12-pulse diode rectifiers," *IEEE Trans. Power Electron.*, vol. 23, no. 3, pp. 1270–1277, May 2008.
[39] N. R. Raju, A. Daneshpooy, and J. Schwartzenberg, "Harmonic cancellation for a twelve-pulse rectifier using DC bus modulation," in *Proc. IEEE Ind. Appl. Conf. 37th IAS Annu. Meeting*, 2002, pp. 2526–2529.
[40] M. E. Villablanca, J. I. Nadal, F. A. Cruzat, and W. C. Rojas, "Harmonic improvement in 12-pulse series-connected line-commutated rectifiers," *IET Power Electron*, vol. 2, no. 4, pp. 466–473, Jul. 2009.
[41] S. Bai and S. M. Lukic, "New method to achieve AC harmonic elimination and energy storage integration for 12-pulse diode rectifiers," *IEEE Trans. Ind. Electron.*, vol. 60, no. 7, pp. 2547–2554, Jul. 2013.
[42] F. Meng, T. Li, L. Wang, and L. Gao, "Series-connected 36-pulse rectifier using a hybrid harmonic injection method," *IET Power Electron,* vol. 13, no. 17, pp. 4112–4116, Dec. 2020.
[43] F. J. Chivite-Zabalza, A. J. Forsyth, and I. Araujo-Vargas, "36-pulse hybrid ripple injection for high-performance aerospace rectifiers," *IEEE Trans. Indus. Appl.*, vol. 45, no. 3, pp. 992–999, May/Jun. 2009.
[44] F. J. Chivite-Zabalza and A. J. Forsyth, "A 48-pulse converter using DC-ripple injection," in *Proc. 7th Int. Conf. Power Electron. Drive Syst.*, 2007, pp. 599–606.
[45] I. Araujo-Vargas, A. J. Forsyth, and F. J. Chivite-Zabalza, "High-performance multipulse rectifier with single-transistor active injection," *IEEE Trans. Power Electron.*, vol. 23, no. 3, pp. 1299–1308, May 2008.

Qingxiao Du was born in Shandong, China, in 1995. She received the B.S degree in electrical engineering from the Harbin Institute of Technology, Weihai, China, in 2017, and the M.S. degree in electrical power engineering from the University of Southampton, Southampton, U.K., in 2018. She is currently working toward the Ph.D. degree in electrical engineering with the Harbin Institute of Technology, Harbin, China.

Her research interests include harmonic elimination and fault analysis on high-power rectifiers.

Lei Gao was born in Hebei, China, in 1982. She received the B.S., M.S., and Ph.D. degrees in electrical engineering from the Harbin Institute of Technology, Harbin, China, in 2005, 2007, and 2012, respectively.

Since 2012, she has been an Assistant Professor with the Harbin Institute of Technology, Weihai, China. Her research interests include power electronics and motor drives.

Quanhui Li was born in Shandong, China, in 1996. He received the B.S and M.S. degrees in electrical engineering in 2018 and 2020, respectively, from the Harbin Institute of Technology, Weihai, China, where he is currently working toward the Ph.D. degree in electrical engineering.

His research interests include multipulse rectifier and high-power rectification.

Wei Liu was born in Shandong, China, in 1997. He received the B.S degree in electrical engineering in 2020 from Harbin Institute of Technology, Weihai, China, where since 2020, he has been working toward M.S. degree in power electronics and power drives.

His research interests include power electronic transformer and power decoupling control.

Xinyu Yin was born in Shandong, China, in 1997. She received the B.S degree in electrical engineering in 2020 from Shandong Agricultural University, Tai'an, China. She is currently working toward the M.S. degree in power electronics and power drives with the Harbin Institute of Technology, Weihai, China.

Her research interests include power electronic transformer and multiple power supply system.

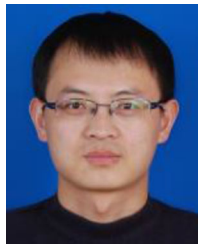

Fangang Meng (Member, IEEE) was born in Shandong, China, in 1982. He received the B.S degree in thermal energy and power engineering in 2005, and the M.S. and Ph.D. degrees in electrical engineering in 2007 and 2011, respectively, from the Harbin Institute of Technology, Harbin, China.

Since 2020, he has been working as a Professor with the Harbin Institute of Technology, Weihai, China. His research interests include harmonic detection, stability analysis of converter and high power rectification.